jmr&t
Journal of Materials Research and Technology
www.jmrt.com.br

Original article

Computational thermodynamic analysis of secondary phases in super ferritic stainless steels

Lorena Braga Moura[a,*], *Hamilton Ferreira Gomes de Abreu*[b], *Yuri Soares Negreiros*[b]

[a] *Department of Industry, Instituto Federal de Educação, Ciência e Tecnologia do Ceará, Fortaleza, CE, Brazil*
[b] *Department of Metallurgical and Materials Engineering, Universidade Federal do Ceará, Fortaleza, CE, Brazil*

ARTICLE INFO

Article history:
Received 29 January 2013
Accepted 1 February 2013
Available online 4 August 2013

Keywords:
Super ferritic stainless steel
Computational thermodynamics
Molybdenum

ABSTRACT

Super ferritic steels belong to a family of steels with Cr content greater than 25% and which also have Mo in their compositions. They were first developed for use in heat exchangers and marine environments. The increase in Mo content in austenitic stainless steels increases the corrosion resistance in mediums that are rich in naphthenic acid or other sulphur complexes. This present work is part of a study for adapting the composition of commercial super ferritic steels by increasing Mo content in the alloy so they can be used in petroleum plants that refine petroleum oils rich in sulphur compounds. We studied the precipitation of phases for experimental compositions of Fe–25Cr–XMo–YNi (X = 5% and 7%; Y = 2% and 4%) with Nb and Ti added. Calculations from the computational program Thermo-Calc were used for the simulation of the phase diagrams and the weight fraction of the phases present. The results from the experimental compositions were compared with those obtained for commercial UNS S44660 super ferritic stainless steel. The stability temperature of the ferritic phase was determined and the possible intermetallic phases were identified in accordance with the temperature variation and chemical composition.

1. Introduction

Ferritic stainless steels are widely used in general industry because they have good mechanical properties and good corrosion resistance [1]. Studies have been published about the effect that increased Mo content has on the resistance to naphthenic corrosion that results from the processing of heavy crude oil [2–5]. The presence of Mo, however, causes the precipitation of intermetallic phases such as the Sigma phase (σ), Chi phase (χ), Mu phase (μ), nitrides like $Fe_5Mo_{13}N_4$, carbides like $(Cr, Fe, Mo)_{23}C_{36}$ or Nb and Ti carbonitrides like Nb(CN) and Ti(CN). The presence of these phases can result in embrittlement with a loss of corrosion resistance at elevated temperatures, and also reduced toughness [6–9].

In previous studies, the performance of AISI 444 ferritic steel was compared with AISI 316L austenitic steel for use in distillation towers. It was found that the AISI 444 had inferior corrosion resistance, but cost less compared to the AISI 316L steel [10]. The composition of AISI 444 steel was modified with

* *Corresponding author.*
E-mail addresses: lorenabraga@ifce.edu.br, lorenabraga@yahoo.com.br (L.B. Moura).
2238-7854 http://dx.doi.org/10.1016/j.jmrt.2013.02.013

the addition of Cr and Mo, and aspects like corrosion resistance, mechanical properties, and formation of the α' phase were studied [11]. The effects of the increase in Cr and Mo on the microstructure and weldability of ferritic steels were also researched. It was observed that an improvement in naphthenic corrosion resistance was accompanied by a loss of toughness [8,12]. Through the addition of Ni, this new proposal aims to improve the toughness without decreasing the naphthenic corrosion resistance. The increase in Ni leads to an increase in Cr content in order to maintain the ferritic matrix. In the search for steels that have better mechanical and metallurgical properties and which can be used efficiently and at a lower cost, super ferritic stainless steels – also known as high performance ferritic stainless steels – are an alternative [13].

The increase in the performance of ferritic stainless steels is achieved with levels of Cr above 25% and Mo additions that improve corrosion resistance in various media. The low levels of C and N improve the ductility, weldability and corrosion resistance, and allow the addition of Ni to improve the toughness. Also, the addition of stabilizing elements such as Nb and Ti hinder the formation of carbides and nitrides and act in the grain refinement [7,13]. These alloys can be used in many corrosive environments, for example, in chemical industries, petroleum refineries, petrochemical industries, food and paper industries, in heat condensers for seawater, and other marine applications [14].

High performance stainless steels are commonly used in environments where chlorides, low pH, or high microbiological activity are present. Elements such as Cr, Mo, and N are known to promote resistance to pitting corrosion in the presence of chlorides [4,15]. It is interesting to note that Ni, which is very common as an alloy element in stainless steels, has little or no effect on resistance to this type of corrosion [15]. Pitting corrosion is highly localized, causes the formation of small holes or points on the surface of the component, has a high propagation rate, and can be completely destructive in terms of useful life of the component [16]. The pitting resistance equivalent (PRE) for stainless steels is often expressed in terms of Eq. (1), developed by Rockel in 1978 and tested by the ASTM G 48-99 [15].

$$\mathrm{PRE} = \%\mathrm{Cr} + 3.3\ \ (\%\mathrm{Mo}) + 16\ \ (\%\mathrm{N}) \quad (1)$$

Good performance in the development of stainless steel depends on a delicate balance between the chemical composition, processing, and type of use, and also the thermodynamic calculation which has become an important approximation tool for understanding the properties of the materials and the processes, benefiting the development of new steels in particular [17]. The use of computational thermodynamics in the commercial computational analysis software Thermo-Calc, together with its databases built according to the CALPHAD protocol which consists of expressing Gibbs' free energy from multicomponent systems through algebraic equations as a function of the pressure, temperature, and chemical composition, allows the phase equilibrium and metastable equilibrium to be calculated, phase diagrams to be constructed, and thermodynamic data to be critically evaluated. It is possible to refine the equation parameters by means of experimental information to predict the properties of ternary, quaternary, and higher order systems with a high degree of accuracy [18,19].

Table 1 – Chemical composition of ferritic stainless steels.

Alloys	Cr	Mo	Ni	C	N	Nb + Ti	Fe	PRE
L1	25	5	2	0.03	0.03	0.6	Equil.	41.98
L2	25	5	4	0.03	0.03	0.6	Equil.	41.98
L3	25	7	2	0.03	0.03	0.6	Equil.	48.58
L4	25	7	4	0.03	0.03	0.6	Equil.	48.58
S44660	27	3.7	1.5	0.015	0.02	0.45	Equil.	39.53

PRE, pitting resistance equivalent.

The objectives of this work are: to study experimental compositions of stainless steels through computational thermodynamics for the purpose of developing high performance ferritic stainless steel alloys; to determine the appropriate thermal processing steps; and to verify the precipitation of intermetallic phases with respect to the variation of chemical composition and temperature. The results obtained with the experimental compositions are compared with the composition of a commercial stainless steel.

2. Materials and methods

Several compositions of ferritic stainless steel with varying percentages of molybdenum and nickel, and addition of niobium and titanium were evaluated. The levels of carbon and nitrogen remained low. Table 1 shows the compositions investigated and the composition of the commercial UNS S44660 super ferritic stainless steel [15,20].

The PRE value was calculated using Eq. (1) and the PRE value for each alloy studied is also available in Table 1.

Using the Thermo-Calc software and the TCFE6 database, the phase diagrams of the proposed compositions were constructed as a function of the variation of the Ni percentage. Also, the weight fraction diagram of each phase was constructed as a function of temperature. The results of the experimental systems were compared with the commercial steel diagrams.

3. Results

The phase diagrams for the experimental alloys and the commercial alloy were constructed in accordance with the chemical composition shown in Table 1. Fig. 1 shows the isopleth of the phase equilibrium diagram for the experimental alloys with a Mo content of 5% (the Ni composition versus temperature varies). The Mo content was then set at 7% to obtain the diagram in Fig. 2. The influence of the Ni and Mo levels can be assessed during the formation of the phases present for temperatures between 400 °C and 1600 °C.

The isopleth of the UNS S44660 steel is shown in Fig. 3. It can be compared with the diagrams of Figs. 1 and 2. These diagrams identify all the possible precipitated phases for a particular composition, without quantifying them.

Quantitative identification of the phases can be assessed by analyzing the graphs of the percentage by weight of each

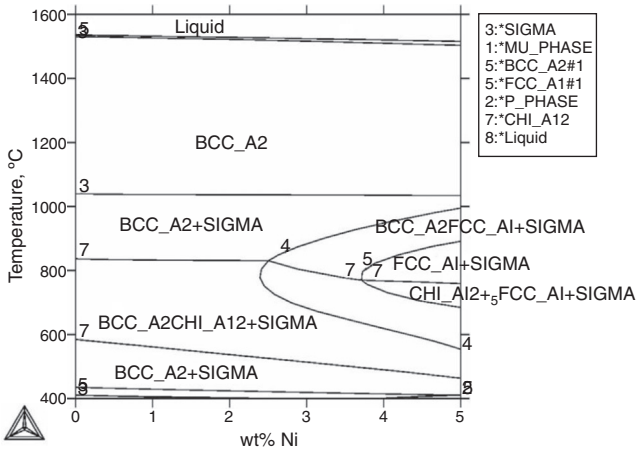

Fig. 1 – Isopleth of the pseudo-binary equilibrium phase diagram for the Fe25Cr5MoNi system.

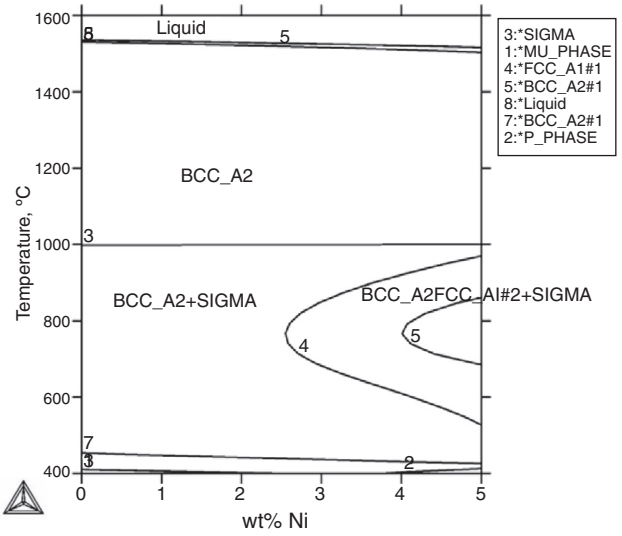

Fig. 3 – Isopleth of the pseudo-binary equilibrium phase diagram for the Fe27Cr3.7MoNi system.

phase as a function of the temperature. The graphs are constructed for each experimental composition and also for the commercial steel. The temperature range at which precipitation occurs for each intermetallic phase can also be observed.

Fig. 4(a and b) compares the influence of varying the molybdenum and nickel percentage in the precipitation of the Chi and Mu phases. The graphs were constructed from data calculated by Thermo-Calc.

Fig. 5(a and b) shows the precipitation of the Sigma phase as a function of the chemical composition. Fig. 6 shows the intermetallic phases precipitated in the commercial alloy.

For the two proposed compositions with nickel content of 4%, stabilization of the CFC phase (face-centered cubic) was observed. The temperature range and the weight fraction of this phase can be seen in Fig. 7.

The approximate solution annealing temperature for each alloy can be estimated by constructing diagrams of weight fraction as a function of temperature – one of these diagrams is shown in Fig. 8 and the solution annealing temperature values for each of the alloys are summarized in Table 2.

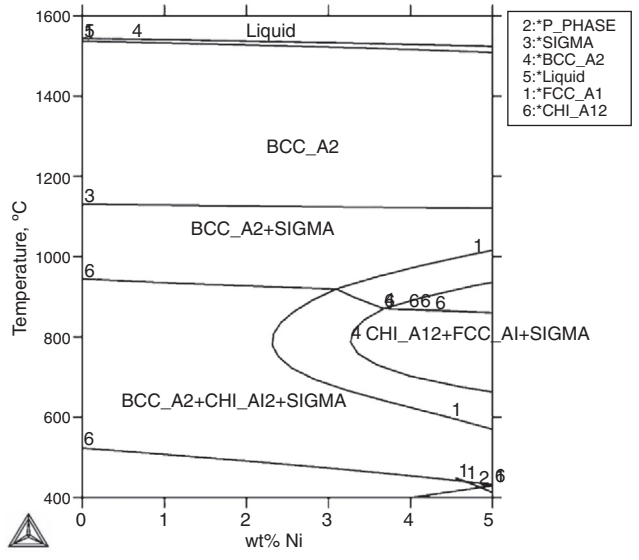

Fig. 2 – Isopleth of the pseudo-binary equilibrium phase diagram for the Fe25Cr7MoNi system.

4. Discussion

In relation to the chemical composition of the experimental alloys shown in Table 1, it can be seen that the increase in Mo content significantly increased the PRE value when compared to the S44660 steel. The high Mo content favors steel passivation by limiting the pitting and naphthenic corrosion [3,4].

The precipitation of sigma (σ), Mu (μ), and Chi (χ) intermetallic phases is thermodynamically favorable for all the compositions studied (Figs. 1 and 2) and also for the commercial UNS S44660 steel (Fig. 3). These phases are diffusional and generally precipitate slowly. The intermetallic phases are characterized as being hard and brittle. The precipitation of these deleterious phases may weaken the steels at certain temperature ranges [6–9]. The formation of these phases can be prevented through heat treatment or high cooling rates after welding [7,9,13]. It can be seen that for temperatures between 600 °C and 1000 °C, precipitation of the CFC phase can occur for Ni content greater than 2% (Figs. 1–3).

Fig. 4(a and b) shows the weight fraction diagrams of the χ and μ phases as a function of temperature and variation of the chemical composition. The χ phase (Fig. 4a) precipitates in the temperature range between 450 °C and 950 °C in all the

Table 2 – Solution annealing temperature.

Alloys	Temperature (°C)
25Cr–5Mo–2Ni	1040
25Cr–5Mo–4Ni	1040
25Cr–7Mo–2Ni	1150
25Cr–7Mo–4Ni	1150
UNS44660	1000

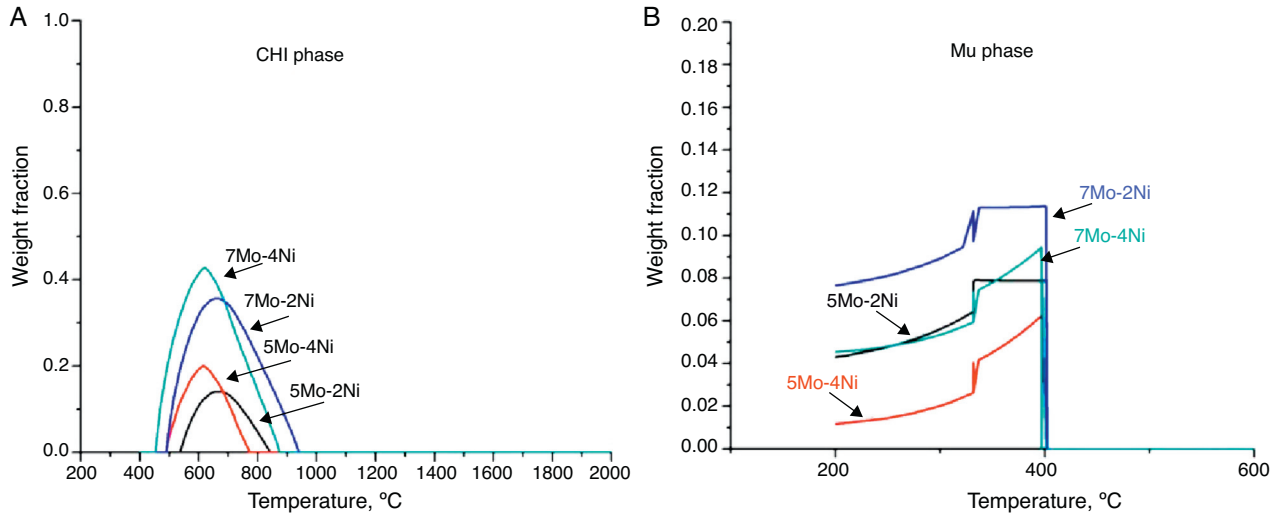

Fig. 4 – Weight fraction of the Chi phase (a) and the Mu phase (b) as a function of temperature, for the experimental alloys.

experimental alloys, with a maximum percentage by weight of 42% for the 7Mo–4Ni alloy at 600 °C. The elevation of the Mo content from 5% to 7% causes an increase of 20% in the percentage by weight for phase χ, while the increase of Ni content from 2% to 4% causes an increase of only 5% in this phase. Moreover, the dissolution temperature of this phase is higher for the alloys with higher Mo content. The μ phase (Fig. 4b) can be seen at temperatures below 410 °C for all the compositions studied. The percentage of the μ phase increases with an increase in Mo content and a reduction in Ni content. The highest percentage by weight for the μ phase occurs for the 7Mo–2Ni alloy with approximately 11% at a temperature of 400 °C. The χ and μ phases are favored by the presence of molybdenum. The kinetics of the phases is related to the temperature and exposure time [9].

The amount of the sigma phase precipitated (Fig. 5) shows that the dissolution temperature of the σ phase increases from 1000 °C to 1100 °C with an increase in the Mo content from 5% to 7%, but variation of the Ni content does not influence the precipitation temperature of this phase. The amount of the σ phase precipitated increases with the increase in Mo and Ni content, reaching a maximum of 60% of the σ phase for the 7Mo–4Ni alloy at a temperature of 900 °C.

For the commercial steel (Fig. 6), the precipitated intermetallic phases are μ and σ, in the same temperature range as for the experimental alloys with 5% Mo. The weight fraction of the μ phase is approximately 8% at 400 °C and the σ phase attains a maximum of 52% at approximately 700 °C. Precipitation of phase χ does not occur in the UNS S44660 steel, probably due to the lower Mo content in these steels. The CFC phase that appears as thermodynamically favorable in the phase diagram (Fig. 3) shows a percentage of less than 1% when analyzing the weight fraction. Thus, the χ and CFC phases are identified in the isopleth of the phase diagram, as well as the Laves phase and some nitrides, but they do not appear in considerable quantity in the weight fraction

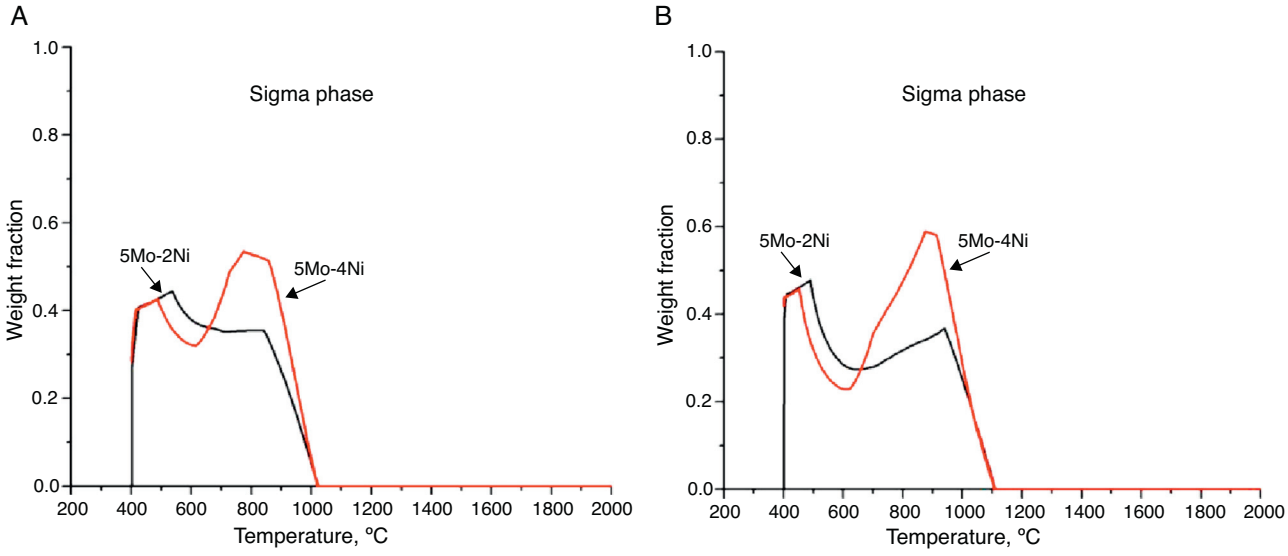

Fig. 5 – Weight fraction of the Sigma phase as a function of the temperature, for the experimental alloys.

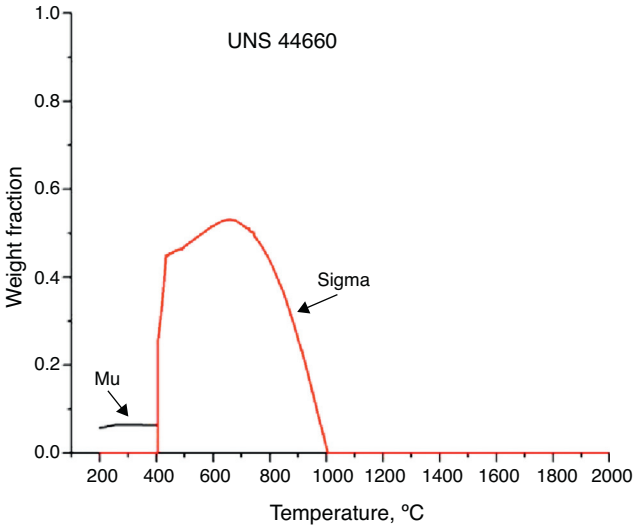

Fig. 6 – Weight fraction of the Sigma and Mu phases as a function of the temperature, for the UNS44660 steel.

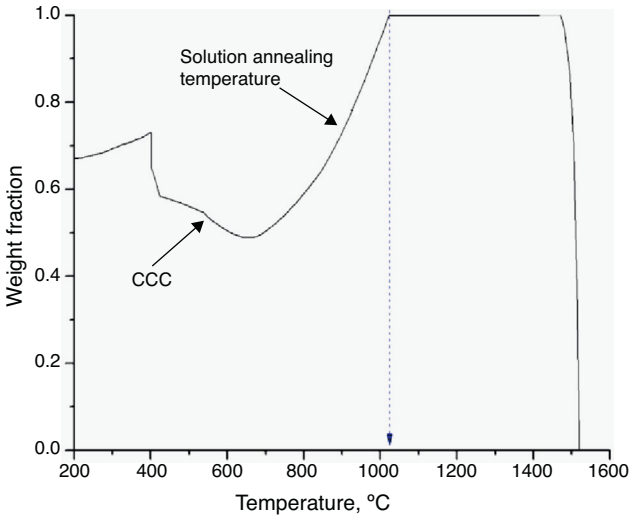

Fig. 8 – Identification of the solution annealing temperature for the 5Mo–2Ni alloy.

diagram. A more thorough study on the kinetics of precipitation is needed for these phases.

The phase diagrams calculated in Figs. 1 and 2, and the alloys with 2% Ni show stabilization of the ferritic phase for all the evaluated temperatures, while for the alloys containing 4% Ni it is observed that, besides the presence of the ferritic phase, there is stabilization of the CFC phase in the temperature range between approximately 600 °C and 1000 °C. The quantification of this stage is shown in Fig. 7. The increase in Mo content reduces the percentage of the CFC phase which attains a maximum weight fraction of 50% for the 5Mo–4Ni alloy at 850 °C. The improved toughness in ferritic stainless steels is related to the quantity of interstitial elements (like C and N), grain size, amount of Ni, and heat treatment. The experimental alloys have low interstitials and stabilizing elements (Nb and Ti) that were added to promote grain refinement. The increase in Ni content favored the stabilization of the CFC

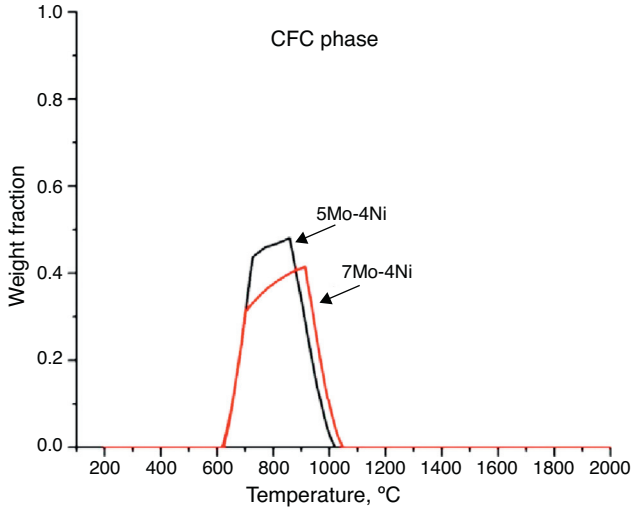

Fig. 7 – Weight fraction of the CFC phase as a function of the temperature, for the experimental alloys with 4% Ni.

phase in the alloys with lower Mo content. It can cause the formation of martensite during the rapid cooling for temperatures between 600 °C and 1000 °C, which can be resolved by a heat treatment for solubilization.

Associating the composition with the heat treatment for solution annealing that is suitable for the alloys with water cooling can prevent the formation of deleterious or unwanted phases [7,13]. The solution annealing temperature of the ferritic matrix can be determined from graphs of the weight fraction as a function of temperature (Fig. 8). The increase in Mo content increases the solution annealing temperature of the experimental alloys, but the Ni content exerts no influence. The alloys with 5% Mo solubilize at 1040 °C, while for the alloys with 7% Mo this temperature increases to 1150 °C. For the UNS S44660 steel, the solution annealing temperature is 1000 °C. High solution annealing temperatures not only promote homogeneity of the microstructure, but also favor growth of the grain of the matrix. A microstructural study of the alloys is necessary.

More detailed studies on the precipitation kinetics of the intermetallic phases and formation of the CFC phase are planned for future research. Ingots have already been melted with the four compositions that were thermodynamically analyzed and this will be the subject of studies to compare the experimental data with those calculated using Thermo-Calc.

5. Conclusions

1. All the experimental alloys showed PRE values higher than the commercial alloy.
2. The increase in Mo content caused the appearance of the intermetallic Chi (χ) phase and increased the percentage of the μ and sigma phase.
3. With the increase in Ni content there was a reduction in the percentage of the μ phase, but the σ and χ phases increased.
4. The alloys with 4% Ni content have between 30% and 50% weight fraction for the CFC phase between 600 °C

and 1000 °C. The optimal operating temperature should be maintained below 600 °C to avoid CFC precipitation.

5. The solution annealing temperature increases with the increase in Mo content, but it is not influenced by varying the Ni content.
6. Kinetic study of phase transformation is necessary for better understanding of these alloys.

REFERENCES

[1] Smith WF. Structure and properties of engineering alloys. 2nd ed. New York: McGraw-Hill; 1993.

[2] Baptista IP, Jóia CJBM, Fontes RGM, Carvalho LJ. Sistema e metodologia de avaliação da corrosividade naftênica em laboratório. In: Conferência sobre tecnologia de equipamentos. Proceedings of the 7th COTEQ Conference. 2003. p. 8.

[3] Gallo G, Edmondson J. The effect of molybdenum on stainless steels and naphthenic acid corrosion resistance. In: NACE International, Organizer. Proceedings of the Corrosion congress. 2008. p. 13.

[4] Negreiros YS, Herculano LFG, Lima-Neto P, Araujo WS, Guimarães RF, Abreu HFG. Efeito do teor de Mo na resistência a corrosão de ligas FeCrMo. In: Congresso Brasileiro de Engenharia e Ciência dos Materiais. Proceedings of the 18th CBCiMat Congress. 2008.

[5] Vasconcelos IF, Tavares SSM, Reis FEU, Abreu HFG. Ageing effects on α' precipitation and resistance to corrosion of a novel Cr–Mo stainless steel with high Mo content. J Mater Sci 2009;44:293–9.

[6] Park CJ, Ahn MK, Know HS. Influence of Mo substitution by W on the precipitation kinetics of secondary phases and the associated localized corrosion and embrittlement in 29%Cr ferrite stainless steels. Mater Sci Eng 2006;418:211–7.

[7] Andrade TF, Kliauga AM, Plaut RL, Padilha AF. Precipitation of Laves phase in a 28%Cr–4%Ni–2%Mo–Nb superferritic stainless steel. Mater Charact 2008;59:503–7.

[8] Guimarães RF. Efeito do teor de Mo na microestrutura de juntas soldadas em ligas FeCrMo. Fortaleza: Universidade Federal do Ceará; 2011 [D.Sc Tesis].

[9] Moura LB, Guimarães RF, Abreu HFG, Miranda HC, Tavares SSM. Naphthenic corrosion resistance, mechanical properties and microstructure evolution of experimental Cr–Mo steels with Mo content. Mater Res 2012;15:277–84. Available from: http://www.scielo.br/pdf/mr/ahead/aop_0942-11.pdf [Internet].

[10] Souza JA, Abreu HFG, Nascimento AM, Paiva JAC, Lima-Neto P, Tavares SSM. Effects of low-temperature aging on AISI 444 steel. J Mater Eng Perform 2005;14:367–72.

[11] Reis FEU. Influência do alto teor de Mo na microestrutura de liga Fe–Cr. Fortaleza: Universidade Federal do Ceará; 2007 [M.Sc. dissertation].

[12] Moura LB. Influência do teor de Cr e Mo na microestrutura e na textura de liga FeCrMo. Fortaleza: Universidade Federal do Ceará; 2010 [M.Sc. dissertation].

[13] Kovak CW. High performance stainless steels. USA: Nickel Development Institute; 2011 [Cited 2012, February 19]. Available from: http://www.nickelinstitute.org/TechnicalLiterature/Reference%20Book%20Series/HighPerformanceStainlessSteels_11021_.aspx

[14] Olubambi PA, Potgieter JH, Cornish L. Corrosion behaviour of superferritic stainless steels cathodically modified with minor additions of ruthenium in sulphuric and hydrochloric acids. Mater Des 2009;30:1451–7.

[15] Janikowski D, Blessman E. Super-ferritic stainless steels – the cost-effective answer for heat transfer tubing. In: NACE International, Organizer. Proceedings of the Corrosion Conference. 2008. p. 16.

[16] Llewellyn DT, Hudd RC. Steels metallurgy and applications. 3rd ed. Butterworth: Heinemann; 1998.

[17] Ågre J. Thermodynamic and kinetic modeling of stainless steels past and future trends. In: The Swedish Steel Producers' Association, Organizer. Proceedings of the 6th European Stainless Steel Conference. 2008. p. 245–52.

[18] Garzón CM, Tschiptschin AP. Modelamento termodinâmico e cinético por meio do método CALPHAD do processamento térmico e termoquímico de aços. Rev Mater 2006;11:70–87.

[19] Anderson J-O, Helander T, Hoglung L, Shi P, Sundman B. Thermo-Calc and Dictra, computational tools for materials. Calphad 2002;26:273–312.

[20] Davis Jr, editor. ASM specialty handbook: stainless steels, vol. 2. ASM International; 1994. p. 576.